Nuclear Engineering and Design 278 (2014) 310–316

Nuclear Engineering and Design

journal homepage: www.elsevier.com/locate/nucengdes

Oxidation effect on steel corrosion and thermal loads during corium melt in-vessel retention

V.S. Granovsky[a], V.B. Khabensky[a], E.V. Krushinov[a], S.A. Vitol[a], A.A. Sulatsky[a], V.I. Almjashev[a], S.V. Bechta[b], V.V. Gusarov[c], M. Barrachin[d], P.D. Bottomley[e,*], M. Fischer[f], P. Piluso[g]

[a] *Alexandrov Scientific-Research Technology Institute (NITI), Sosnovy Bor, Russia*
[b] *KTH, Stockholm, Sweden*
[c] *SPb State Technology University (SPbGTU), St. Petersburg, Russia*
[d] *Institut de Radioprotection et de Sûreté Nucléaire (IRSN), St Paul lez Durance, France*
[e] *EC-Joint Research Centre, Institute for Transuranium Elements (ITU), Karlsruhe, Germany*
[f] *AREVA GmbH, Erlangen, Germany*
[g] *Commissariat à l'Energie Atomique et aux Energies Alternatives (CEA), Cadarache, St Paul lez Durance, France*

HIGHLIGHTS

- The METCOR facility simulates vessel steel corrosion in contact with corium.
- Steel corrosion rates in UO_{2+x}–ZrO_2–FeO_y coria accelerate above 1050 K.
- However corrosion rates can also be limited by melt O_2 supply.
- The impact of this on in-vessel retention (IVR) strategy is discussed.

ARTICLE INFO

Article history:
Received 7 April 2014
Received in revised form 23 July 2014
Accepted 28 July 2014

ABSTRACT

During a severe accident with core meltdown, the in-vessel molten core retention is challenged by the vessel steel ablation due to thermal and physicochemical interaction of melt with steel. In accidents with oxidizing atmosphere above the melt surface, a low melting point UO_{2+x}–ZrO_2–FeO_y corium pool can form. In this case ablation of the RPV steel interacting with the molten corium is a corrosion process.

Experiments carried out within the International Scientific and Technology Center's (ISTC) METCOR Project have shown that the corrosion rate can vary and depends on both surface temperature of the RPV steel and oxygen potential of the melt. If the oxygen potential is low, the corrosion rate is controlled by the solid phase diffusion of Fe ions in the corrosion layer. At high oxygen potential and steel surface layer temperature of 1050 °C and higher, the corrosion rate intensifies because of corrosion layer liquefaction and liquid phase diffusion of Fe ions.

The paper analyzes conditions under which corrosion intensification occurs and can impact on in-vessel melt retention (IVR).

1. Introduction

IVR is a part of the severe accident management strategy for several light-water reactor designs (Kymalainen et al., 1997; Theofanous et al., 1997; Rogov et al., 1996; Fischer and Levi, 2010; Oh et al., 2006; Dinh et al., 2004). Leaving out reactivity accidents, the RPV being cooled can in principle fail under the effect of thermal and mechanical loads or because of the wall melt-through. In Kymalainen et al. (1997) and Theofanous et al. (1997) the RPV failure conditions are studied, such as failure under the thermal shock conditions or failure caused by thinning of the wall which is partially melted under the influence of the heat flux transferred to the wall from the melt and depending on residual heat and molten pool structure. Results of the study show that one of the main conditions required for the IVR is efficient external cooling of the RPV for preventing the wall melt-through. To achieve this condition, the heat flux from vessel outer surface to coolant water should not exceed a

* Corresponding author. Tel.: +49 7247 951 364; fax: +49 7247 951 593.
E-mail address: paul.bottomley@ec.europa.eu (P.D. Bottomley).

http://dx.doi.org/10.1016/j.nucengdes.2014.07.034

critical value (critical heat flux) for the whole surface being cooled. This paper addresses only conditions for in-vessel retention of fully oxidized corium melt.

In general, thinning of the RPV wall can be a result of both melting and physicochemical interaction between melt and RPV steel. In Bechta et al. (2008a, 2009) it was shown that with this interaction and in the above-melt air and steam atmosphere, the steel ablation follows an oxidation mechanism, and correlations for the corrosion rate have been proposed. In the following study Bechta et al. (2008b) the related thinning of the vessel wall in addition to its partial melting was shown that the vessel integrity of VVER reactor was not jeopardized so long as a small thickness of outer, cooled vessel wall was retained of full mechanical strength.

The current paper presents new experimental results obtained within the ISTC METCOR Project, which studied the influence of melt oxygen potential on the vessel steel corrosion and will analyze conditions where corrosion can influence the heat flux transferred from the melt to the RPV wall, DNB margin, and, consequently, IVR conditions.

2. Interaction of molten corium with steel under high oxygen potentials of the melt

Experimental investigations of the cooled vessel steel corrosion in molten corium under air and steam atmospheres was carried out by the NITI team for IVR-typical conditions using test facilities of the RASPLAV platform within the ISTC METCOR Project. A 1.5–2.0 kg corium pool was generated on top of vessel steel specimen by induction heating in a cold crucible.

The MC10 and MCP-2 experiments were performed with high liquidus temperature ("refractory") corium-type UO_{2+x}–ZrO_2; MC1, MC2, MC11, MC12, and MCP-4 experiments – with lower liquidus temperature ("fusible") corium – UO_{2+x}–ZrO_2–FeO_y (where $x \leq 0.2$ in METCOR conditions). For comparison the 50 mol% UO_2–50 mol% ZrO_2 has a solidus/liquidus temperature of around 2500 °C (Lambertson and Mueller, 1953) while the 40 mol% UO_{2+x}–40 mol% ZrO_2–20 mol% FeO has a solidus temperature of ~1340 °C (Almjashev et al., 2010). All experiments except MCP-4 were performed with samples of Russian VVER reactor steel 15Kh2NMFA, experiment MCP-4 was performed with a sample of European reactor steel 20MNMONI 5-5. In all the experiments identical procedures were used for the experiment and post-test analysis, as described in Bechta et al. (2008a, 2009).

Figs. 1 and 2 show the induction furnace and RPV steel specimen, respectively.

Each experiment included several 'quasi-stationary' regimes of gradually increasing specimen surface temperature. After reaching a certain temperature the specimen-corium system was held at these conditions for a predetermined period of time, during which the specimen corrosion depth was measured by the ultrasonic scanning method. The duration of this period depended on the corrosion rate. The fact is that the larger corrosion depth, the more accurately corrosion rate can be determined, but the more difficult it is to maintain a stable temperature of the specimen surface (and heat flux into the specimen) because this temperature tends to decrease with an increase in corrosion depth. Therefore, the higher the corrosion rate, the shorter the 'quasi-stationary' regime. After completion of a period, the melt-specimen heat flux was increased either by a higher power deposition in the melt (rise in melt temperature) or by moving either the crucible (7, Fig. 1) or the electromagnetic screen (17) compared to the inductor (8), i.e. with change in Zc, Ze (Fig. 1).

The corium composition was the same in all the experiments except MCP-4. In MCP-4 (Fig. 3) the first three temperatures (1005, 1130, 1200 °C – stages 1, 2 & 3) correspond to the conditions of

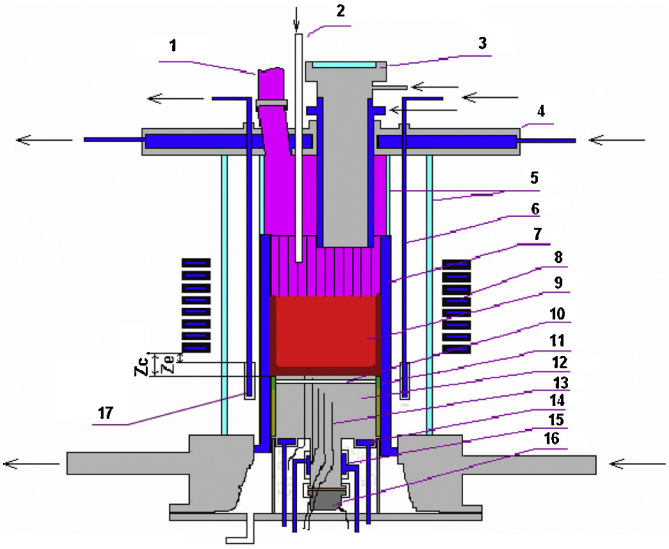

Fig. 1. Diagram of the induction furnace. (1) Gas and aerosol out; (2) air or steam in; (3) pyrometer shaft; (4) lid; (5) quartz tubes; (6) EM screen hanger tube; (7) crucible sections; (8) inductor; (9) melt; (10) acoustic defect; (11) ZrO_2 insulation; (12) vessel steel specimen; (13) K-type thermocouples; (14) top calorimeter of the specimen; (15) bottom calorimeter of the specimen; (16) ultra-sonic sensor (USS); (17) EM screen.

specimen interaction with refractory corium. After that the temperature on the steel specimen surface was lowered, iron was added into the melt, and after its oxidation during next three temperature levels (920, 1080, 1150 °C – stages 4, 5 & 6) steel corrosion at the interaction with fusible corium was investigated.

Upon completion of each experiment, the electromagnetic heating was disconnected and the melt was allowed to crystallize. The ingot was then cooled in steam or air. The posttest analysis included a series of physicochemical studies of the specimen and corium ingot, as well as the numerical modeling of specimen temperature conditions.

The experimental corrosion rate data were interpreted using the model based on the Tamman equation (Tamman, 1920) and the Arrhenius law. It was assumed that: (i) the corrosion rate is controlled by the transport of Fe^{2+} ions from the steel surface through the corrosion layer and corium crust, which presents the main diffusion barrier, (ii) the oxygen content in the melt is in excess and allows Fe oxidation to FeO – the main component of corrosion layer, and that the oxygen content does not influence the corrosion rate (Bechta et al., 2008a, 2009).

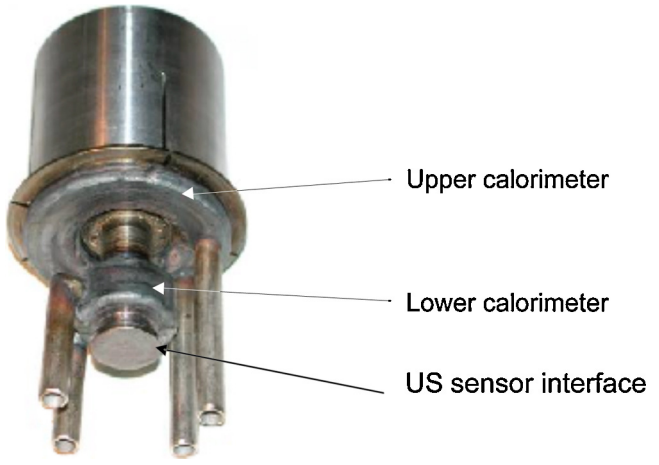

Fig. 2. Vessel steel specimen.

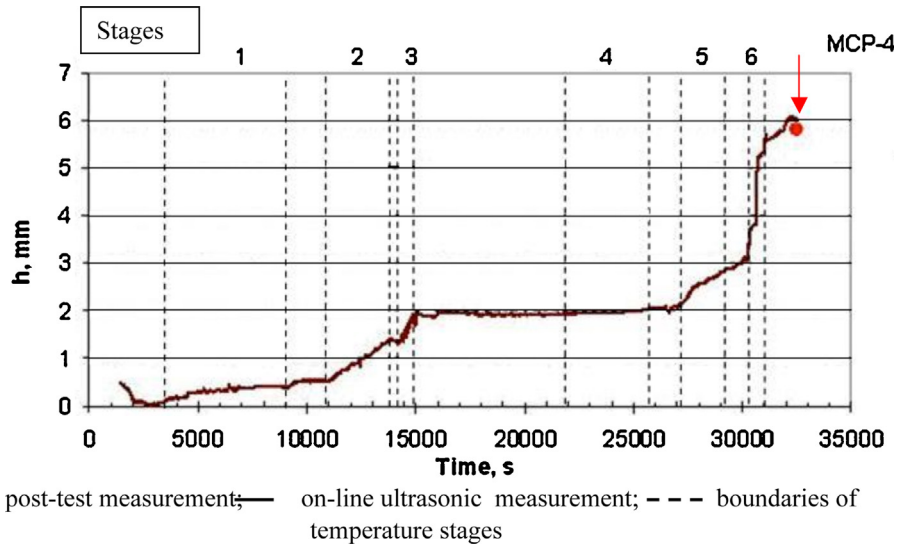

Fig. 3. Specimen corroded thickness versus time in MCP-4.

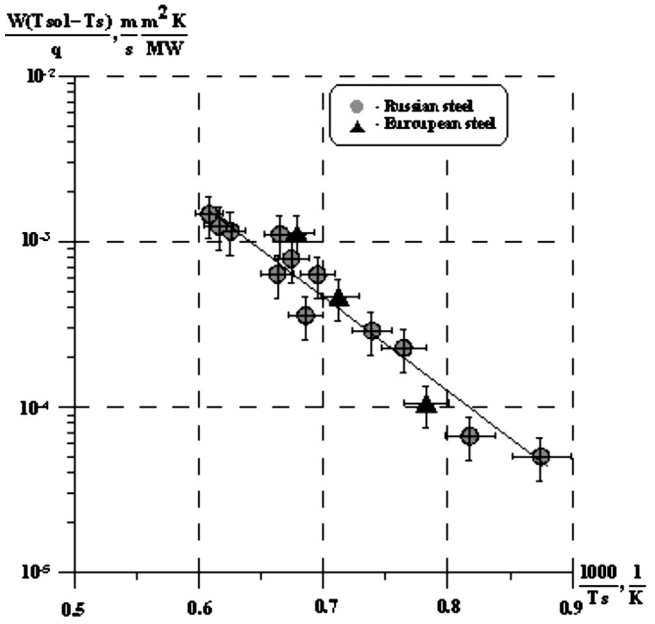

Fig. 4. Oxidation kinetics of vessel steel during its interaction with the "refractory" UO_{2+x}–ZrO_2 corium melt.

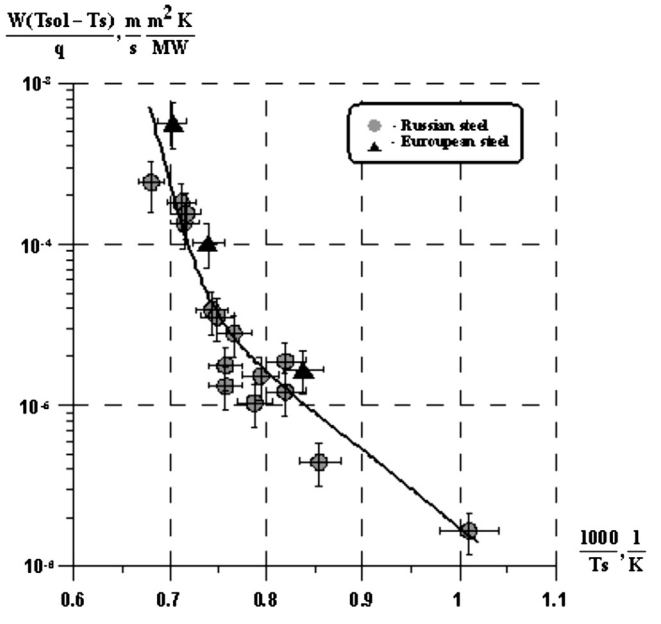

Fig. 5. Oxidation kinetics of vessel steel during its interaction with the "fusible" UO_{2+x}–ZrO_2–FeO_y corium melt.

Figs. 4 and 5 give the summarized experimental data on the corrosion of Russian steel for the refractory and fusible corium respectively (Bechta et al., 2008a, 2009).

Correlations for the corrosion rate of the Russian VVER vessel steel (Bechta et al., 2009) are as follows:

UO_{2+x}–ZrO_2 coria

$$\frac{W(2723 - T_S)}{q} = 4.98 \exp\left(-\frac{1.1 \times 10^5}{RT_S}\right), \quad (1)$$

UO_{2+x}–ZrO_2–FeO_y coria

$$\frac{W(1613 - T_S)}{q} = 0.1 \exp\left(-\frac{0.91 \times 10^5}{RT_S}\right) + 3.4 \times 10^{14} \exp\left(-\frac{4.99 \times 10^5}{RT_S}\right), \quad (2)$$

where W – corrosion rate, m/s; T_s – temperature of steel surface, K; q – heat flux from molten corium to steel, MW/m^2; R – universal gas constant, J/(mol K); correlations (1) and (2) with all comments can be found in Bechta et al. (2009).

It follows from Figs. 4 and 5 that the data for European reactor steel can be approximately described by the same correlations (1) and (2). However the number of tests with European steel is quite limited and would need further investigations. For the "fusible corium", it was observed that corrosion intensifies when the steel surface temperature exceeds approximately 1050 °C ($1000/T_S < 0.75$). Results of SEM/EDX analysis were used (Bechta et al., 2008a) to explain this by partial liquefaction of the solid corrosion layer (Almjashev et al., 2010) and, consequently, by accelerated Fe^{2+} liquid-phase diffusion through the corium crust. Note that the experimental results including an observed increase in the corrosion rate were obtained for non-oxygen-deficient corium conditions.

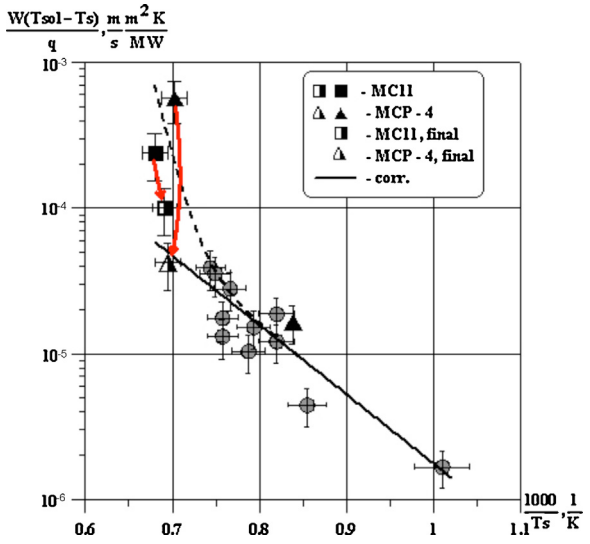

Fig. 6. Kinetics of steel corrosion at its interaction with fusible corium at the Fe^{2+} solid-phase diffusion, with arrows showing the shift from initial (intensified) to final (reduced) corrosion rates in the final stages of the MC11 and the MCP4 tests.

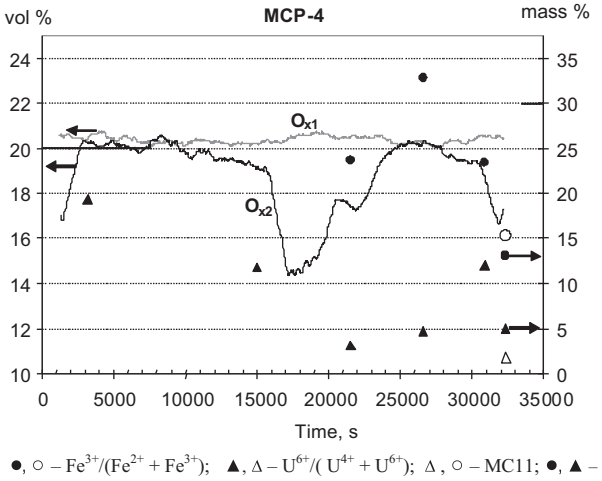

●, ○ – $Fe^{3+}/(Fe^{2+} + Fe^{3+})$; ▲, Δ – $U^{6+}/(U^{4+} + U^{6+})$; Δ, ○ – MC11; ●, ▲ – MCP-4

Fig. 7. a) Oxygen concentration (vol.%) in the in- and off-gases (O_{x1} & O_{x2}, resp.) and b) Fe^{3+} and U^{6+} mass fractions: ●, ○ – $Fe^{3+}/(Fe^{2+} + Fe^{3+})$; ▲ Δ – $U^{6+}/(U^{4+} + U^{6+})$ mass%, respectively (●, ▲ MCP-4 samples; Δ, ○ single MC11 sample).

3. Steel corrosion at the reduction of melt oxygen potential

In two experiments with fusible corium: MC11 – Russian steel, steam atmosphere above the melt and MCP-4 – European steel, air atmosphere above the melt, an interesting observation was made. After the period of intensive corrosion at the last maximum temperatures (two leftmost points in Fig. 5), before disconnecting the heating, the corrosion rate decreased. In experiment MCP-4 the slowdown of corrosion is observed during the last 6th temperature stage in Fig. 3 at approximately from 31,000 to 31,800 s (before the inductor disconnection – see arrow). Similar data for MC11 are given in Bechta et al. (2008a).

The summarized data on steel corrosion and its interaction with fusible corium are given in Fig. 6 where all points are shown in Fig. 5 except 4 points in $1000/T_s < 0.75$ region; here only two points are shown (MC11 – Fig. 6 uses symbols different from those in Fig. 5, & MCP-4) are shown in this region: both in high-rate corrosion period and subsequent slow-rate corrosion period (marked as final). It can be seen that initial points related to the pre-slowdown period in Fig. 5 (for MCP-4 – stage 6, Fig. 3) are described by the correlation, which takes intensified corrosion into account (the process of liquid-phase diffusion), and points indicated as "final" in Fig. 6 (for MCP-4 – period between completion of stage 6 and turning the inductor off, Fig. 3) are located closer to the correlation for the solid-phase diffusion extrapolated to the high temperature region $1000/T_s < 0.75$ (Fig. 5).

Since the high-rate corrosion of RPV steel leads to rapid thinning of the RPV wall and is accompanied by additional heat production, it can be considered as a negative factor and it seems important to determine a possible reason for the observed corrosion slowdown. For this purpose let us consider the measured data on the oxygen content in the MCP-4 melt (not measured in other experiments) and the history of measured oxygen concentrations in the furnace off gases (O_{x2}) shown in Fig. 7. When interpreting this curve, the additional uncertainty due to the delay of the "gas" measurement – time losses due to transport in gas line and inertia (capacity) of the gas volume in the furnace should be considered. In the same figure there are points, which denote experimental kinetics of Fe^{3+} and U^{6+} fractions from $(Fe^{2+} + Fe^{3+})$ and $(U^{4+} + U^{6+})$ contained in the melt, respectively. These data are produced by the chemical analysis of melt samples taken during the experiment and at the final state from the ingot.

Evident is the sharp reduction of oxygen concentration in off gases (O_{x2}) in comparison with its concentration in the supplied air (O_{x1}), i.e. the oxygen is absorbed by the melt approximately after 15,000 s, when iron is added to the melt (to change its composition). It is explained by the loss of equilibrium (in terms of oxygen) between furnace atmosphere and the melt due to the oxidation of introduced iron. The melt oxygen potential is also decreased at this point, (U^{6+} fraction is reduced). The same effect is observed from approx. 30,000 s on, i.e. during the 6th stage. This decrease can be explained by the high temperature oxidation rate of steel surface, i.e. oxygen spent on the steel oxidation is not compensated for by its supply into the melt from the atmosphere.

The most representative data characterizing the oxygen potential of the melt at the end of stage 6 are obtained thanks to post-test analyses of the final state in the ingot (in Fig. 7 two MCP-4 points of U^{6+} and Fe^{3+} fractions produced by the ingot average sample are shown at ~32,500 s). It can be seen that U^{6+} fractions and, especially Fe^{3+} fractions, according to this sample are lowest in the final state than those of the samples taken on line during the experiment. The model in Bechta et al. (2008a, 2009), used to analyze the experimental data, assumes a constant oxygen potential in atmosphere and unlimited exchange of oxygen between atmosphere and melt i.e. unchanged oxygen potential in the melt under conditions of equilibrium with the atmosphere. Under these conditions the only limiting mechanism for the corrosion rate is the Fe^{2+} diffusion through the corrosion layer and corium crust, but not the transport of O^{2-} ions from the melt to the steel specimen surface. But there are deviations from equilibrium in melt oxygen potential with the atmosphere as seen in Fig. 7 because a decrease of oxygen potential in the melt, provoked a rapid corrosion. Therefore, the diffusion transport of O^{2-} ions becomes limited and that this is likely to cause the corrosion rate reduction.

In MC11, similar to other experiments on steel corrosion with the oxidizing above-melt atmosphere (excluding MCP-4), the composition of off-gases was not measured and melt samples were not taken during the experiment, so the value of oxygen potential in the melt at the final stage can be derived only from the ingot composition. Chemical analysis of the ingot average sample of fractions of Fe^{3+} and U^{6+} from the total ions of iron $(Fe^{2+} + Fe^{3+})$ and uranium $(U^{4+} + U^{6+})$ were 15.1% and 1.5%, respectively. They were close to the values measured for the MCP-4 ingot (in Fig. 7 these are the concentrations plotted at ~32,500 s). For this reason, as in MCP-4, the deviation of the considered point from the correlation can be attributed to the reduction of oxygen potential in the melt. Note

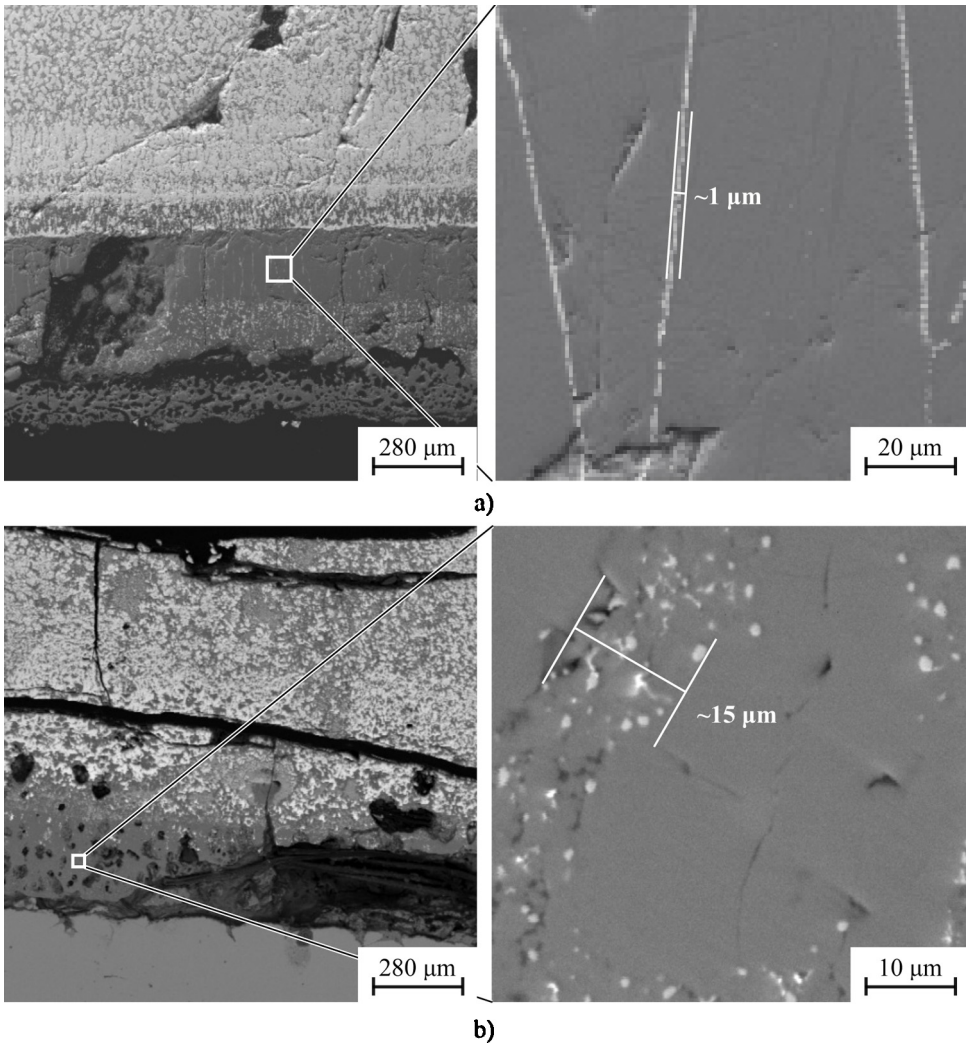

Fig. 8. SEM-images of corrosion layer: (a) experiment MCP-4; (b) experiment MC12.

that since MC11 was conducted with the steam atmosphere above the melt, so probably the production of hydrogen has also an impact on oxygen potential.

In order to understand the mechanism of oxygen potential influence on corrosion rate we shall compare the MCP-4 SEM/EDX data for the corrosion layer on the steel surface with those of MC12 experiments (Russian steel, fusible corium, air) (Bechta et al., 2008a). Note that in MC12, like in MC11, intensive steel corrosion was observed during the last regime, but, differently from MC11, heating was disconnected during the intensive corrosion of steel specimen and corium solidification was made.

Fig. 8a shows SEM-images of the MCP-4 corrosion layer. Fig. 8b shows similar results of MC12 (Bechta et al., 2008a) for comparison. The figures demonstrate qualitative structural difference of corrosion layers: in MC12 the inter-granular eutectic layer (~10 μm) is much wider than in MCP-4 (~1 μm). It can be assumed that this reflects a different character of diffusion processes: the prevailing diffusion in liquid state in MC12 and diffusion in solid state in MCP-4.

These results enable us to presume that the corrosion rate reduction with decrease of oxygen potential in the melt reveals itself only (or mostly) by the lower liquid-phase diffusion through the corrosion layer. Thus the liquid-phase diffusion itself, main factor of steel corrosion, governs the increase of oxygen consumption, the reduction of oxygen potential in the melt and then, eventually, corrosion slowdown. Therefore, in the MCP-4 and MC11 experimental conditions self-suppression of the intensive, liquid-phase-based corrosion regime took place.

4. Impact of vessel steel corrosion in the IVR conditions

Let us consider the influence of vessel steel corrosion on the IVR for a situation in which a molten pool of fully oxidized fusible corium with high oxygen potential was formed in the lower head before the melt – vessel interaction starts. If, under these conditions, the temperature on the interaction interface increases to levels at which a solid crust will completely melt that is, the steel interacts with liquid corium directly; then we can assume that the corrosion rate grows rapidly and that the reactor vessel temperature increase will be determined by this steel oxidation reaction.

As shown in a number of works dedicated to the IVR analysis, e.g. Kymalainen et al. (1997) and Theofanous et al. (1997), in parts of the reactor bottom the heat flux entering the inside vessel surface will lead to local melting. Here corrosion rates can be very high and, in extreme cases, corrosion can be further enhanced by the so-called liquid-phase burning mechanism, i.e. *exothermic redox reaction on the surface of the two-liquid interface* (Gusarov et al., 2007).

The model of liquid-phase burning was developed for the conditions of suboxidized melt interaction with oxidic sacrificial material (SM) of the core catcher (Sulatsky et al., 2005). The ceramic SM

consists mostly of Fe_2O_3 and Al_2O_3, of 70 and 30 mass%, respectively. In the thin reaction layer on the SM surface, Zr contained in the melt reacts with Fe_2O_3. The heat of chemical reaction is spent on the SM heating and melting and, partially, transferred to the melt. Heat transfer from the reaction layer is performed by the free convection heat exchange.

In IVR conditions, that are different from those of the model, the reducing agent is the vessel steel and the oxidizing agent is the oxygen contained in the melt; but this difference does not change the model substantially. Heat from the redox reaction is released in the thin reaction layer on the steel surface. This heat is partially transferred to the steel surface, and partially – to the corium melt, where the heat is transferred by the mechanism of free convection. In the applied model, it is further considered that now a part of the heat transferred to the steel surface is conducted through the steel into the cooling water, while this heat loss can be neglected in the case of a ceramic SM because of its low thermal conductivity.

Heat flux transferred to steel wall in the unsteady state heat conduction equation including melting is determined using model correlations (Sulatsky et al., 2005). As the steel wall thickness decreases by melting, heat flux transferred from the wall to the water increases, heat consumption for melting decreases and, consequently, melting rate and heat production rate in the reaction layer decrease, and eventually liquid phase burning goes out.

The following conditions were chosen for numerical analysis:

- The 0.18 m-thick steel wall has the initial temperature of 100 °C. Temperature on the cooled outer surface does not change with time. The steel melting temperature is 1500 °C and the oxidic melt temperature is 2200 °C (liquidus temperature is ~1900 °C). Heat flux from oxidic melt to the wall before the start of liquid-phase burning is 0.6 MW/m^2.
- Heat effect during steel oxidation is assumed to be equal to the heat release from the exothermal redox reaction conventionally taking place at 2200 °C – $U_3O_8 + 2Fe = 3UO_2 + 2FeO$ (80 kJ/mole Fe). The higher degree of U oxidation (to U_3O_8 or $UO_{2.66}$) for IVR conditions in comparison with $UO_{2.2}$ for METCOR conditions) is explained by the effect of high steam-air pressure in the reactor and containment on thermodynamic equilibrium concentration of oxygen in the melt before melt-RPV steel interaction starts.
- The mass fraction of molten steel (μ) taking part in the redox reaction within the reaction layer is varied between 0 and 1. $\mu = 1$ means that all melted RPV steel participates in oxidation reaction within the reaction layer. $\mu = 0$ means that all melted RPV steel is oxidized outside the reaction layer and, thus, there is no liquid phase burning.
- The problem is solved numerically in the 1D formulation.

Figs. 9 and 10 show the kinetics of the unablated vessel thickness and heat flux from the cooled surface versus time. The larger the μ value is, the thinner is the unablated vessel part and the higher is the maximum heat flux value. In absence of heating caused by steel oxidation ($\mu = 0$ in Fig. 9) the thickness of the unablated vessel part at the 0.6 MW/m^2 heat flux is 0.072 m. When ablation stops ($\mu > 0$), the oxidic crust is formed on the internal wall surface, and the heat flux reduces to the specified value 0.6 MW/m^2.

It can be seen that at $\mu > 0.5$ in Fig. 10 the resulting heat flux reaches the level of the critical heat flux q_{cr} (for the vertical surface in the large volume of saturated water at P = 0.1 MPa, $q_{cr} \approx 1.2$ MW/m^2).

However, as shown in Section 3, the high-rate corrosion of steel can lead to a decrease in the oxygen potential of the melt which inhibits corrosion. Let us consider the possibility of this effect for IVR conditions.

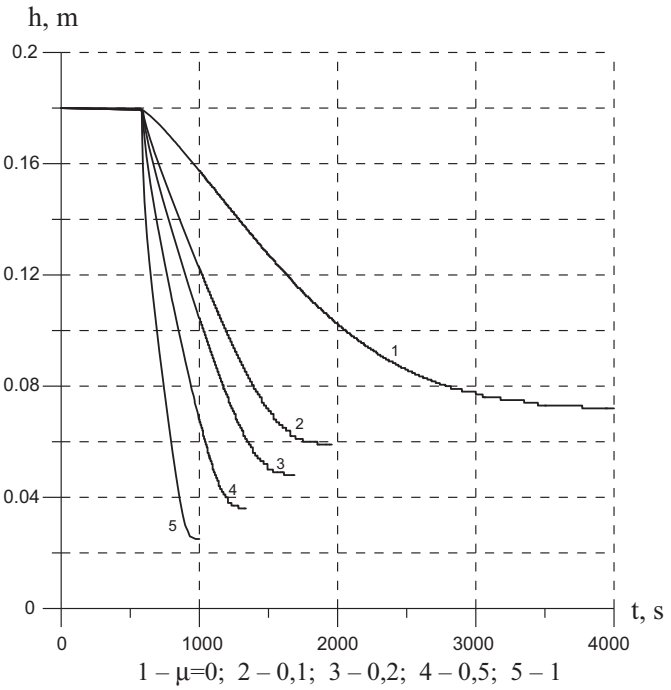

Fig. 9. Thickness of steel wall during liquid-phase burning versus time for various metal mass fraction ratios (μ).

Decrease of melt oxygen concentration caused by steel corrosion versus time is as follows

$$\frac{dC_{O2}}{dt} = \frac{1}{M_{corium}}(G_{O2}S_{up} - kW_{corrosion}S_{corrosion});$$

where C_{O2} – oxygen concentration in the melt; M_{corium} – melt mass, kg; G_{O2} – flow-rate of oxygen coming into the melt, kg/s; $W_{corrosion}$ – corrosion rate, m/s; $k = \rho_{Fe}\,\mu_O/\mu_{Fe}$, kg/M^3; ρ_{Fe} – Fe density, kg/m^3;

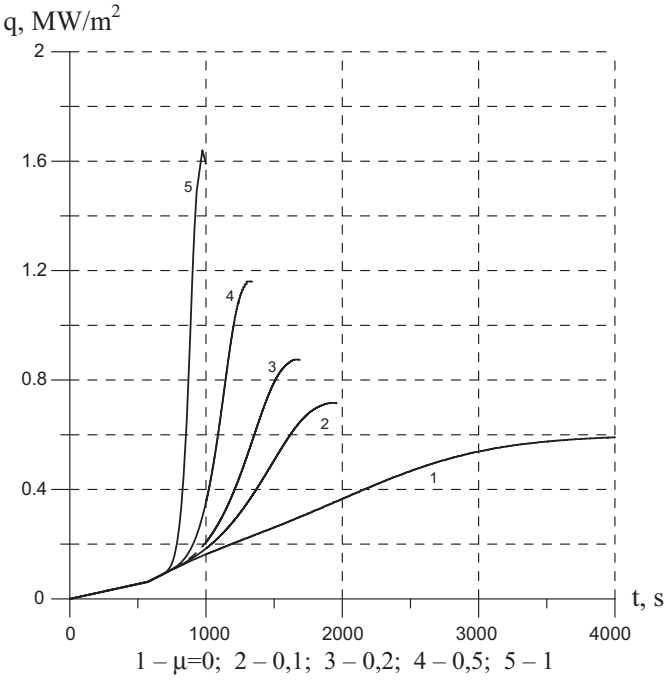

Fig. 10. Heat flux during liquid-phase burning versus time for various metal mass fraction ratios (μ).

μ_O, μ_{Fe} – atomic weights of O and Fe, kg/kmole; S_{up} – area of corium top surface, M^2; $S_{corrosion}$ – area of corrosion surface, m^2.

It is obvious that other conditions being equal, the lower M_{corium} and G_{O2} and higher $S_{corrosion}$ are, the smaller ablation depth is at which the oxygen concentration in the melt and, consequently, the degree of U oxidation reduces to a limit at which a high corrosion rate is no longer possible. Results in Fig. 7 show that $UO_{2.06}$ ($U^{6+}/(U^{4+}+U^{6+}) \approx 15\%$) is this limiting value. Since the ablation depth clearly correlates with the heat flux to the cooling water (Figs. 9 and 10), the heat flux will not achieve its maximum value if the limiting (minimum) degree of U oxidation is reached earlier than the maximum ablation depth is reached.

It is not easy to evaluate the current importance of the issues addressed in this paper, however, it seems advisable to consider the possibility of high corrosion rates of RPV steel and also conditions for its inhibition in IVR analyses in view of multiple scenarios of severe accident development and challenges of their numerical simulations.

5. Conclusions

(1) The effect of corrosion acceleration was investigated in the METCOR project and has already been identified and correlations for refractory (UO_2–ZrO_2) and fusible (UO_2–ZrO_2–FeO) coria proposed in earlier publications. In this publication, further evaluation of these experiments has noted a decrease in the corrosion rate and liquid phase 'burning' effects have been additionally calculated for these IVR conditions.

(2) We note that the corrosion 'acceleration' studied under METCOR was due to the formation of low-melting liquid phases at grain boundaries; this is different from the liquid phase "burning" due to exothermic release from metallic melt oxidation at the interface.

(3) A slowing down of the corrosion rate has been observed and appears to be due to reduced diffusional supply of oxygen to the interface from the corium atmosphere interface. This indicates that oxygen potential in the melt could affect the corrosion rate at the interface and that many factors could influence the melt potential and hence the corrosion rate.

(4) The vessel steel corrosion phenomena of a fusible corium melt in the IVR conditions primarily depend on the probability of fully oxidized corium layer formation in the bottom of molten pool. Such a situation is likely to occur either in large loss-of-coolant accidents, where the steam–gas mixture from the containment appears in the reactor vessel, or where water enters the reactor vessel (e.g. resulting from operator's action). Given that full oxidation is possible but not certain, it is advisable, first, to extend the temperature range of experiments on the vessel steel corrosion up to the steel melting temperature and, second, to study the oxidation kinetics of the melt itself at different O_2 potentials on its interface. These experimental results can also refine the computational models.

Acknowledgement

This work has been partially funded by the European Commission through the International Science and technology Center (ISTC) within the contract No. 3592.

References

Almjashev, V.I., Barrachin, M., Bechta, S.V., et al., 2010. Phase equilibria in the FeO_{1+x}–UO_2–ZrO_2 system in the FeO_{1+x}-enriched domain. J. Nucl. Mater. 400 (2), 119–126.

Bechta, S.V., Granovsky, V.S., Khabensky, V.B., et al., 2008a. Interaction between molten corium UO_{2+X}–ZrO_2–FeO_Y and VVER vessel steel. In: Proc. ICAPP'08, Paper 8052, Anaheim, CA, USA, June 8–12.

Bechta, S.V., Khabensky, V.B., Krushinov, E.V., et al., 2008b. VVER steel corrosion during in-vessel retention of corium melt. In: Proc. ERMSAR-2008, Bulgaria.

Bechta, S.V., Granovsky, V.S., Khabensky, V.B., et al., 2009. VVER vessel steel corrosion at interaction with molten corium in oxidizing atmosphere. Nucl. Eng. Des. 239, 1103–1112.

Dinh, T.N., Tu, J.P., Theofanous, T.G., 2004. Two-phase natural circulation flow in AP-1000 in-vessel retention-related ULPU-V facility experiments. In: Proc. ICAPP'04, Pittsburgh, USA.

Fischer, M., Levi, P., 2010. The severe accident control strategy of the KARENA™ BWR. In: Proc. ICAPP'10, San Diego, CA, USA, p. 10165.

Gusarov, V.V., Almjashev, V.I., Khabensky, V.B., et al., 2007. Physicochemical simulation of the combustion of materials with the total endothermal effect. Glass Phys. Chem. 33 (5), 492–497.

Kymalainen, O., Tuomisto, H., Theofanous, T.G., 1997. In-vessel retention of corium at the Loviisa plant. Nucl. Eng. Des. 169, 109–130.

Lambertson, W.A., Mueller, M.H., 1953. Uranium oxide phase equilibrium systems: III. UO_2–ZrO_2. J. Am. Ceram. Soc. 36, 365–368.

Oh, S.J., Parc, K.C., Kim, H.G., 2006. Advanced design features of APR 1400 and realization in Shin Kori construction project. In: Proc. ICAPP'06, Reno, USA.

Rogov, M.F., Loginov, S.A., Granovsky, V.S., et al., 1996. Analyzing the possibility of retaining the corium in the vessel of a VVER-640 reactor in a severe accident with a damage core. Therm. Eng. 43 (11), 888–892.

Sulatsky, A.A., Bechta, S.V., Granovsky, V.S., et al., 2005. Molten corium interaction with oxidic sacrificial material of VVER core catcher. In: Proc. ICAPP'05, Paper 5240, Seoul, Korea, May 15–19.

Tamman, G., 1920. Uber Anlauffarben von Metallen. Z. Anorg. Allg. Chem. B 111 (H1.5), 78–89.

Theofanous, T.G., Lin, C., Addition, S., et al., 1997. In-vessel coolability and retention of a core melt. Nucl. Eng. Des. 169, 1–48.